Temporal imaging with a high filling-factor

Avi Klein,[1] Inbar Sibony,[1] Sara Meir,[1] Hamootal Duadi,[1] Michelle Y. Sander,[2] and Moti Fridman[1, a)]
[1)]*Faculty of Engineering and the Institute of Nanotechnology and Advanced Materials, Bar-Ilan University, Ramat Gan 5290002, Israel*
[2)]*Department of Electrical and Computer Engineering, Boston University, 8 Saint Mary's Street, Boston, MA 02115, USA*
Photonics Center, Boston University, 8 Saint Mary's Street, Boston, MA 02115, USA
Division of Materials Science and Engineering, Boston University, 15 Saint Mary's Street, Brookline, MA 02446, USA

(Dated: 11 June 2021)

We demonstrate a temporal imaging system that can capture events with unknown time-of-arrival in the time domain without the need to synchronize the signal. The temporal imaging system is based on a time-lens that uses a high repetition-rate fiber laser for the pump wave together with a time-stretch scheme. After dispersion, the timing between adjacent pump pulses is smaller than the pulse width. Therefore, the signal interacts with one of the pump pulses with high probability, regardless of its arrival time. We discuss the intensity dependence and temporal aberrations of such an imaging system and demonstrate a direct temporal imaging of the build-up dynamics of solitons.

The equivalent between diffraction of light in free space and dispersion of pulses as they propagate in dispersive materials has led to the invention of novel temporal imaging schemes[1–4]. These temporal imaging schemes can image and capture short signals in time[5], they can magnify or compress them[6], and map their optical spectrum to the time domain and vice versa[7].

Temporal imaging schemes are based on time-lenses which induce a quadratic phase shift in time. This is the equivalent to spatial lenses based on geometric diffraction which induce a quadratic phase shift in space. The first demonstrated time-lenses were based on electro-optical modulators that are limited in speed[1–4]. We focus on time-lenses that are based on the four-wave mixing process which is a fast process and can impose the quadratic phase on the signal via a nonlinear interaction with a pump wave[8,9]. These time-lenses can induce larger phase-shifts over short time periods, leading to stronger time-lenses than possible with electro-optics modulators[9–13]. With these time-lenses, we demonstrated different types of temporal imaging schemes[14–20] and utilized them to measure and investigate rare ultrafast events[21,22].

However, since such time-lenses rely on the interaction between the incoming signal wave and a tailored pump wave, it is crucial to synchronize the pump wave with the incoming signal wave. Only when both the signal and pump waves overlap in time, they can interact and generate the idler wave. Thus, it is challenging to overlap the pump pulses with signals that have unknown time-of-arrival and image them in time. Different methods to overcome this drawback were presented, such as time-stretch schemes which measure the signal continuously but only the optical spectrum and not the temporal pulse characteristics[23–25]. Another technique increased the repetition rate of the signal wave, but it is not suitable for imaging single-shot events[26].

To overcome this synchronization challenge, we developed a high filling-factor temporal imaging system, which can image single-shot signals without the need to synchronize them to a pump wave and combine it with time-stretch measurements. The main principle behind this temporal imaging system is to utilize a high repetition-rate ultrafast laser for the pump wave of the time-lens, so that after dispersion the temporal gap between adjacent pump pulses is smaller than the pulse width. Therefore, when a signal wave enters the time-lens, it will interact with one of the pump pulses with high probability, regardless of its time-of-arrival. The time-stretch measurement indicates the arrival timing of the signal compared to the time-lens which enables to compensate for the pump intensity profile and to take into account the temporal aberrations of imaging with the edge of the lens. Finally, we utilized the system for investigating the build-up dynamics of solitons with high resolution. Our system is similar to temporal schemes with multiple time-lenses which were presented by us[14,18–20] and others[27,28]. However, in all of those systems the arrays of time-lenses were limited in time since there were longer dark periods without a pump wave between adjacent arrays. Further, these temporal imaging scheme had a filling factor of less than 1%, while here we demonstrate a continuous array of time-lenses with a high filling-factor of more than 50%.

Similar high repetition-rate time-lenses were developed for analyzing 160 Gb/s input signals by Fourier transforming the input signal[29]. While this system had time-lenses with high repetition-rate, similar to our idea, the system was engineered solely for Fourier transform without the ability to obtain high magnification of ultrashort signals and only for incoming bits with known time-of-arrival. This was necessary for obtaining specific wavelengths for each channel. However, in our system, we developed a temporal imaging system with large magnification, high filling-factor, and high temporal resolution, which we combined with time-stretch measurements, for investigating ultrafast signals with unknown time-of-arrival.

Our system is schematically shown in Fig. 1. A custom-designed erbium-doped fiber laser with a 3 nm bandwidth a 1 ps temporal width, and a peak power of $1kW$, serves as a pump laser. The pump wave is provided by a high repetition-rate ultrafast laser based on a soliton mode-locking in conjunction with a semiconductor Bragg reflector as a saturable

[a)]Electronic mail: Mordechai.fridman@biu.ac.il

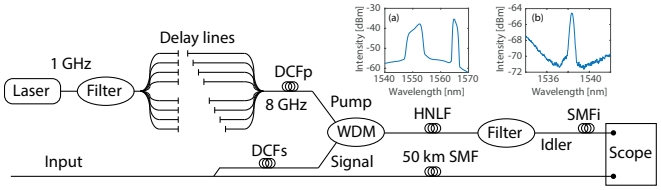

FIG. 1. Schematic of a high filling-factor temporal imaging system based on a 8 GHz repetition-rate time-lens combined with a time-stretch measurement. Lengths of the fibers in the system: DCFp = from 100 m to 500 m; DCFi = from 50 m to 250 m; HNLF = 500 m; SMFi = 5 km. The dispersion of the DCF (Thorlabs DCF38) is about $-38 ps/nm/km$, the dispersion of the SMF (Corning SMF-28) is about $18 ps/nm/km$, and the dispersion of the HNLF (ofs HNLF zero-slope) is negligible. (a) Measured spectrum of the pump (1553 nm) and signal (1565 nm) waves. (b) Measured spectrum of the generated idler wave.

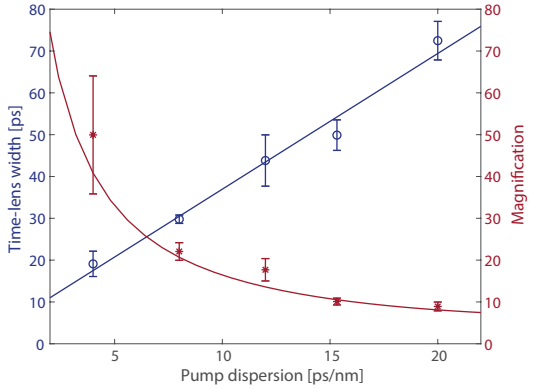

FIG. 2. Measured (dots and circles) and calculated (solid lines) results of the width and magnification of a time-lens as a function of the dispersion of the pump.

absorber[30–34]. The total cavity length of this linear laser is $10 cm$ leading to a repetition-rate of $1 GHz$[34,35]. This initial pump pulse sequence is multiplied with splitters and free-space delay lines to obtain an 8 GHz pulse train.

The 8 GHz pulse train is sent to the time-lens serving as the pump wave, where each pump pulse generates a single time-lens. The pulse duration compared to the separation between them sets the filling-factor of our system. A higher filling-factor means that when an input signal arrives it has a higher probability to interact with a pump pulse while a lower filling-factor implies that the input signal can potentially be missed. On the other hand, the amount of dispersion sets the power of the time-lens and its F-number. A smaller accumulated dispersion value leads to a higher F-number and stronger time-lens[1,3]. So, when designing the high filling-factor time-lens scheme, there is a trade-off between choosing a higher dispersion for wider time-lenses leading to a higher filling-factor on one hand, or a smaller dispersion for a higher F-number leading to a larger magnification on the other hand.

To demonstrate this trade-off, we designed time-lenses with five different values of focal distances by replacing the dispersion fibers for the pump and signal waves. Specifically, we replaced the pump fiber, DCFp, to be 50, 100, 150, 200 and 250 m, while replacing the signal fiber, DCFs, to be half the length of DCFp to maintain imaging conditions. Then we measured the duration of each time-lens and its magnification when considering the same dispersion values for the signal and idler waves. The results are presented in Fig. 2 together with the numerical calculations showing a good agreement between the experimental measurements and the theoretical predictions. The time-lens width increased linearly from 20 ps to 70 ps, by increasing the pump dispersion, which increased the filling-factor. However, the magnification of the time-lens decreased, as illustrated in Fig. 2 from a maximum magnification of 50 to a value smaller than 10.

Next, we maximized the time-lens width to obtain the highest filling-factor possible by our system, while working with a temporal magnification around 10. With this system, we temporally-imaged a pulse train of 3 ps with a bandwidth of 1 nm and a repetition-rate of 100 MHz. Since the repetition-rate of the input signal differs from the pump pulse sequence of the time-lenses, each input pulse arrived asynchronously with a different timing compared to the high filling-factor time-lens pulses. By comparing the number of pulses imaged by the time-lenses to the number of pulses generated by the laser, we found that over 70% of the input pulses were imaged indicating a filling-factor of over 0.7.

In addition to the time-lens which images the intensity as a function of time, a time-stretch measurement system was added. The input signal was temporally dispersed by passing through a 50 km long fiber and then detected by a high speed photodetector connected to a fast oscilloscope. Thus, the recorded measurements at the oscilloscope represents the optical spectrum of each pulse of the input signal based on the dispersive Fourier transform[23–25]. The two complementary measurements of the dispersed spectrum and the temporal image are shown in Fig. 3(a) where the dashed blue curve denotes the dispersive Fourier spectrum and the solid red curve denotes the temporal image of the input signal. The spectrum of the input signal has a simple Gaussian shape with 2 nm width at half maximum, corresponding to a Gaussian pulse of 2 ps. Each signal pulse interacts with a different part of the dispersed pump and therefore generates an idler at a different wavelength. This specific wavelength which propagates through the 50 km of SMF, leads to a different timing compared to the spectrum measurement. Also, given the temporal pump pulse profile, signals which interacted with the center of the pump pulse generated idler waves with higher intensity than signals which interacted with the off-center parts of the pulse. Therefore, the intensity of the idler waves maps the intensity distribution of the pump as a function of time. We evaluated the intensity of the image, I, as a function of the signal offset compared to the pump timing $\Delta\tau$. The results are shown in Fig. 3(b), showing a Gaussian like shape which is identical to the pump pulse intensity distribution. The Gaussian is maximized at 2 ns and not 0 ns due to differences in the fiber lengths of the time-lens detector and the time-stretch detector. By comparing the time-lens and the time-stretch measurements, we obtained the offset between the signal and the center of the time-lens and, thanks to the pump intensity map-

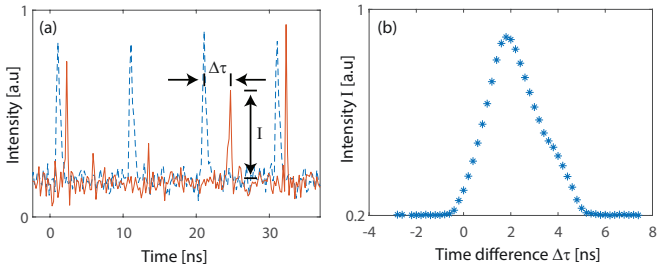

FIG. 3. Temporal imaging of an ultrafast pulse train at a 100 MHz repetition rate by our temporal imaging system. (a) Solid red curve - temporal image of the input pulses by the high filling-factor time-lens scheme; dashed blue curve - spectrum measurement by the time-stretch scheme. (b) The intensity of the high filling-factor time-lens output as a function of the timing difference between the time-lens output and the spectral measurement with the time-stretch scheme.

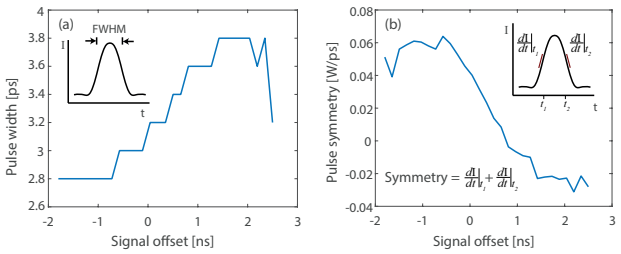

FIG. 4. Temporal aberrations of the imaging system as a function of the signal offset compared to the time-lens center. (a) The output FWHM pulse, shown in the inset, is related to the second order aberrations. (b) The output pulse symmetry, namely the difference between the slopes as shown in the inset, is related to the third order aberrations.

ping, we compensate for the differences in the pump intensity.

We measured the pulse width and symmetry as a function of the signal offset compared to the time-lens center which relates to the temporal aberrations of the imaging system. The second order aberrations increase the width of the pulse while the third order aberrations influence the pulse symmetry[36]. Fig. 4(a) presents the width of the pulse at FWHM where the stairs-like shape is due to our temporal resolution limit. Fig. 4(b) evaluates the symmetry of the pulse by comparing the intensity slope at the two sides of the pulse, where the correct slope is 0.22 W/ps and the aberrations are less than 0.04 W/ps. The results reveal that the left side of the time-lens (negative signal offset) has negligible second and third orders aberrations while the right side of the time-lens (positive signal offset) has higher aberrations. By detecting the signal offset compared to the time-lens center, we can compensate for the pump intensity profile and can take into account the temporal aberrations[37].

Next, we utilized our temporal imaging system for measuring directly the build-up dynamics of solitons. The solitons showed rich dynamics in different systems including soliton exploding, pulsing, and breathing[38–42]. The soliton dynamics in fiber lasers are especially important since these govern the various ultrafast operating regimes[43]. Soliton dynamics were

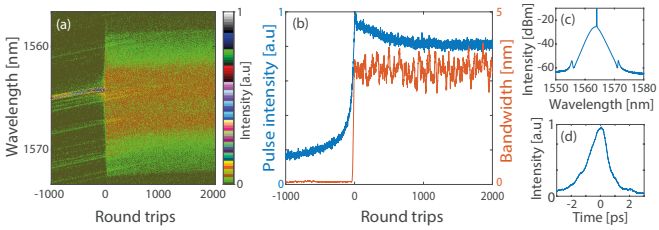

FIG. 5. Spectral measurements of the soliton build-up with the time-stretch system. (a) Measured output spectrum after each round-trip showing the soliton build-up at round-trip 0. (b) Pulse intensity and spectral bandwidth of the laser output as a function of the round-trip number. (c) Spectral measurement of such a soliton by an optical spectrum analyzer. (d) Cross-correlation measurement of such a soliton, indicating a temporal width of 900 fs.

investigated in fiber-lasers so far either in a direct measurement with low temporal resolution[43,44] or with a time-stretch scheme which retrieved only the spectrum[45–48].

We generated solitons in a fiber laser cavity and measured their build-up dynamics. We measured the spectrum of the soliton with a time-stretch configuration and the intensity with our temporal imaging scheme after each cavity round-trip. The time-stretch measurements confirmed similar trends that were previously observed by Peng and Zeng[48]. However, as the time-stretch scheme only measures the spectral intensity, the spectral phase was lost, which can lead to uncertainty in the reconstructed dynamics. With our temporal imaging system, we observed directly the build-up dynamics of solitons and compared the evolution to the retrieved spectrum. The time-stretch results are shown in Fig. 5 where the measured spectrum of the laser output is plotted in Fig. 5(a) after each round-trip. We denote the start of the soliton build-up as round-trip number 0. The laser output intensity and bandwidth as a function of the round-trip number are shown in Fig. 5(b). We also show in Fig. 5(c) and (d) the typical spectrum and cross correlation measurements of the soliton taken with an optical spectrum analyzer and a cross-correlator.

In parallel to the time-stretch measurements, we measured the soliton build-up process with our temporal imaging system. For detecting the temporal shape of each soliton with a sub picosecond temporal resolution, we traded off the filling factor for increased temporal magnification. Due to the reduced filling factor, we detected each pulse every 15 round-trips, which continues to provide a higher filling-factor than previously temporal imaging system with large magnification. Representative results are shown in Fig. 6 where we observe the evolution of the pulse build-up. In the inset, we show the pulse at 200 round-trips before the soliton build-up, the pulse during the build-up process, and 500 round-trips after the build-up process. These results show the width of the pre-soliton pulse at around 15 ps while the soliton has a width of 3 ps.

To conclude, we developed a temporal imaging system with a high filling-factor of 0.7 which can image signals without the need to synchronize them to a pump wave. We discussed the different considerations for designing such a temporal imag-

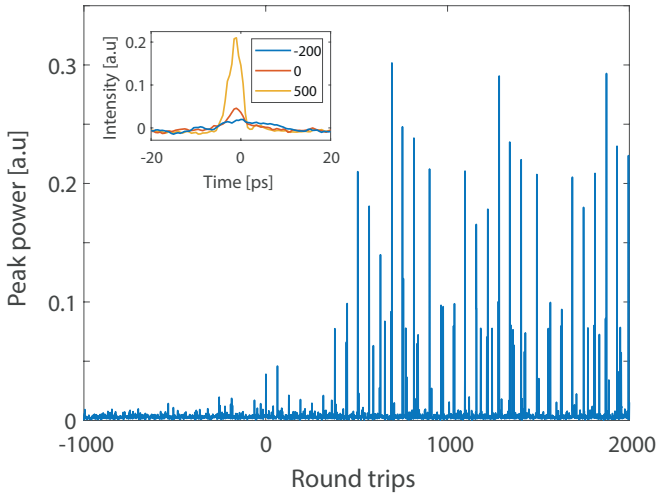

FIG. 6. Temporal imaging measurement of the soliton build-up in an ultrafast fiber laser. The inset shows zoom-in of three representative pulses before, during and after the soliton build-up process.

ing scheme regarding the magnification and filling-factor of the time-lens and considered the pump intensity profile and the temporal aberrations. Finally, we demonstrated our temporal imaging system by directly measuring the build-up dynamics of solitons with high temporal resolution. Our results indicate that current investigations of ultrafast events with the time-stretch method can benefit by our high filling-factor temporal imaging system.

A. Acknowledgements

We would like to acknowledge Junjie Zeng, Boston University, for the development of the GHz fiber laser. Prof. Sander would like to acknowledge the National Science Foundation (ECCS-1710849).

B. Data Availability

The data that support the findings of this study are available from the corresponding author upon reasonable request.

[1] B. H. Kolner and M. Nazarathy, "Temporal imaging with a time lens," Optics letters **14**, 630–632 (1989).
[2] B. H. Kolner, "Space-time duality and the theory of temporal imaging," IEEE Journal of Quantum Electronics **30**, 1951–1963 (1994).
[3] C. V. Bennett and B. H. Kolner, "Principles of parametric temporal imaging. i. system configurations," IEEE Journal of Quantum Electronics **36**, 430–437 (2000).
[4] C. V. Bennett and B. H. Kolner, "Principles of parametric temporal imaging. ii. system performance," IEEE journal of quantum electronics **36**, 649–655 (2000).
[5] N. Berger, B. Levit, S. Atkins, and B. Fischer, "Time-lens-based spectral analysis of optical pulses by electrooptic phase modulation," Electronics Letters **36**, 1 (2000).
[6] M. A. Foster, R. Salem, D. F. Geraghty, *et al.*, "Silicon-chip-based ultrafast optical oscilloscope," Nature **456**, 81–84 (2008).
[7] C. Zhang, B. Li, and K. K.-Y. Wong, "Ultrafast spectroscopy based on temporal focusing and its applications," Selected Topics in Quantum Electronics, IEEE Journal of **22**, 1–12 (2016).
[8] P. Xie, Y. Wen, Z. Wan, X. Wang, J. Liu, W. Yang, X. Li, and Y. Wang, "Electrically tunable temporal imaging in a graphene-based waveguide," Japanese Journal of Applied Physics **58**, 050914 (2019).
[9] R. Salem, M. A. Foster, A. C. Turner, D. F. Geraghty, M. Lipson, and A. L. Gaeta, "Optical time lens based on four-wave mixing on a silicon chip," Optics letters **33**, 1047–1049 (2008).
[10] P. Ryczkowski, M. Närhi, C. Billet, J.-M. Merolla, G. Genty, and J. Dudley, "Real-time full-field characterization of transient dissipative soliton dynamics in a mode-locked laser," Nature Photonics , 1 (2018).
[11] A. Tikan, S. Bielawski, C. Szwaj, S. Randoux, and P. Suret, "Single-shot measurement of phase and amplitude by using a heterodyne time-lens system and ultrafast digital time-holography," Nature Photonics , 1 (2018).
[12] B. Jalali, D. Solli, and S. Gupta, "Silicon photonics: Silicon's time lens," Nature Photonics **3**, 8 (2009).
[13] M. A. Foster, R. Salem, D. F. Geraghty, A. C. Turner-Foster, M. Lipson, and A. L. Gaeta, "Silicon-chip-based ultrafast optical oscilloscope," Nature **456**, 81–84 (2008).
[14] A. Klein, T. Yaron, E. Preter, H. Duadi, and M. Fridman, "Temporal depth imaging," Optica **4**, 502–506 (2017).
[15] M. Fridman, Y. Okawachi, S. Clemmen, M. Ménard, M. Lipson, and A. L. Gaeta, "Waveguide-based single-shot temporal cross-correlator," Journal of Optics **17**, 035501 (2015).
[16] M. Fridman, A. Farsi, Y. Okawachi, and A. L. Gaeta, "Demonstration of temporal cloaking," Nature **481**, 62–65 (2012).
[17] T. Yaron, A. Klein, H. Duadi, and M. Fridman, "Temporal superresolution based on a localization microscopy algorithm," Applied Optics **56**, D24–D28 (2017).
[18] A. Klein, H. Duadi, and M. Fridman, "Full-stokes temporal imaging," Optics letters **43**, 1651–1653 (2018).
[19] A. Klein, I. Sibony, S. Meir, S. Shahal, H. Duadi, and M. Fridman, "Overlapping time-lens array," IEEE Photonics Journal **11**, 3200106 (2019).
[20] H. Duadi, T. Yaron, A. Klein, S. Meir, and M. Fridman, "Phase retrieval by an array of overlapping time-lenses," Optics letters **44**, 799–802 (2019).
[21] A. Klein, H. Duadi, and M. Fridman, "Ultrafast rogue wave patterns in fiber lasers," Optica **5**, 774–778 (2018).
[22] A. Klein, S. Shahal, S. Meir, H. Duadi, K. Sulimany, O. Lib, H. Steinberg, S. A. Kolpakov, and M. Fridman, "Ultrafast twin-peak rogue waves in a vector field," OSA Continuum **2**, 3102–3106 (2019).
[23] K. Goda and B. Jalali, "Dispersive fourier transformation for fast continuous single-shot measurements," Nature Photonics **7**, 102 (2013).
[24] F. Coppinger, A. Bhushan, and B. Jalali, "Photonic time stretch and its application to analog-to-digital conversion," IEEE Transactions on microwave theory and techniques **47**, 1309–1314 (1999).
[25] J. Chou, O. Boyraz, D. Solli, and B. Jalali, "Femtosecond real-time single-shot digitizer," Applied Physics Letters **91**, 161105 (2007).
[26] Y. Okawachi, R. Salem, A. R. Johnson, K. Saha, J. S. Levy, M. Lipson, and A. L. Gaeta, "Asynchronous single-shot characterization of high-repetition-rate ultrafast waveforms using a time-lens-based temporal magnifier," Optics letters **37**, 4892–4894 (2012).
[27] Y. Suen, S. Xiao, S. Hao, X. Zhao, Y. Xiong, and S. Liu, "Time-frequency representation measurement based on temporal fourier transformation," Optics Communications **376**, 86–91 (2016).
[28] X. Zhao, S. Xiao, C. Gong, T. Yi, and S. Liu, "The implementation of temporal synthetic aperture imaging for ultrafast optical processing," Optics Communications **405**, 368–371 (2017).
[29] K. G. Petrillo and M. A. Foster, "Full 160-gb/s otdm to 16x10-gb/s wdm conversion with a single nonlinear interaction," Optics express **21**, 508–518 (2013).
[30] A. E. Akosman, J. Zeng, P. D. Samolis, and M. Y. Sander, "Polarization rotation dynamics in harmonically mode-locked vector soliton fiber lasers," IEEE Journal of Selected Topics in Quantum Electronics **24**, 1–7 (2017).
[31] J. Zeng and M. Y. Sander, "Real-time transition dynamics between multi-pulsing states in a mode-locked fiber laser," Optics Letters **45**, 5–8 (2020).
[32] A. E. Akosman and M. Y. Sander, "Route towards extreme optical pulsation in linear cavity ultrafast fibre lasers," Scientific reports **8**, 13385 (2018).
[33] M. Y. Sander, S. Frolov, J. Shmulovich, E. P. Ippen, and F. X. Kärtner, "10 ghz femtosecond pulse interleaver in planar waveguide technology," Optics

express **20**, 4102–4113 (2012).
[34]J. Zeng, A. E. Akosman, and M. Y. Sander, "Scaling the repetition rate of thulium-doped ultrafast soliton fiber lasers to the ghz regime," Optics express **26**, 24687–24694 (2018).
[35]H. Byun, M. Y. Sander, A. Motamedi, H. Shen, G. S. Petrich, L. A. Kolodziejski, E. P. Ippen, and F. X. Kärtner, "Compact, stable 1 ghz femtosecond er-doped fiber lasers," Applied optics **49**, 5577–5582 (2010).
[36]C. V. Bennett and B. H. Kolner, "Aberrations in temporal imaging," IEEE journal of quantum electronics **37**, 20–32 (2001).
[37]Y. Zhu, J. Kim, and D. J. Gauthier, "Aberration-corrected quantum temporal imaging system," Physical Review A **87**, 043808 (2013).
[38]S. T. Cundiff, J. M. Soto-Crespo, and N. Akhmediev, "Experimental evidence for soliton explosions," Physical review letters **88**, 073903 (2002).
[39]J. M. Soto-Crespo, N. Akhmediev, and A. Ankiewicz, "Pulsating, creeping, and erupting solitons in dissipative systems," Physical review letters **85**, 2937 (2000).
[40]A. Matsko, A. Savchenkov, and L. Maleki, "On excitation of breather solitons in an optical microresonator," Optics letters **37**, 4856–4858 (2012).
[41]X. Yi, Q.-F. Yang, K. Y. Yang, and K. Vahala, "Imaging soliton dynamics in optical microcavities," Nature communications **9**, 3565 (2018).
[42]M. Yu, J. K. Jang, Y. Okawachi, A. G. Griffith, K. Luke, S. A. Miller, X. Ji, M. Lipson, and A. L. Gaeta, "Breather soliton dynamics in microresonators," Nature communications **8**, 14569 (2017).
[43]H. Zhang, D. Tang, L. Zhao, and H. Tam, "Induced solitons formed by cross-polarization coupling in a birefringent cavity fiber laser," Optics letters **33**, 2317–2319 (2008).
[44]A. F. Runge, N. G. Broderick, and M. Erkintalo, "Observation of soliton explosions in a passively mode-locked fiber laser," Optica **2**, 36–39 (2015).
[45]J. Peng, S. Boscolo, Z. Zhao, and H. Zeng, "Breathing dissipative solitons in mode-locked fiber lasers," Science advances **5**, eaax1110 (2019).
[46]K. Krupa, K. Nithyanandan, U. Andral, P. Tchofo-Dinda, and P. Grelu, "Real-time observation of internal motion within ultrafast dissipative optical soliton molecules," Physical review letters **118**, 243901 (2017).
[47]Z. Wang, K. Nithyanandan, A. Coillet, P. Tchofo-Dinda, and P. Grelu, "Optical soliton molecular complexes in a passively mode-locked fibre laser," Nature communications **10**, 830 (2019).
[48]J. Peng and H. Zeng, "Build-up of dissipative optical soliton molecules via diverse soliton interactions," Laser & Photonics Reviews **12**, 1800009 (2018).